International Journal of Heat and Mass Transfer 214 (2023) 124399

Contents lists available at ScienceDirect

International Journal of Heat and Mass Transfer

journal homepage: www.elsevier.com/locate/hmt

Optimizing the trench shaped film cooling design

Lukas Fischer[a,*], Dominik James[a], Sillvya Jeyaseelan[b], Michael Pfitzner[a]

[a] University of the Bundeswehr Munich, Department of Aerospace Engineering, Institute of Thermodynamics, Werner-Heisenberg-Weg 39, Neubiberg 85577, Bavaria, Germany
[b] ENSTA Bretagne, 2 Rue François Verny, Brest 29806, Brittany, France

ARTICLE INFO

Article history:
Received 23 March 2023
Revised 26 May 2023
Accepted 7 June 2023

Keywords:
Film cooling
Computational fluid dynamics (CFD)
GEKO model
Neural network
Bayesian optimization
Heat transfer

ABSTRACT

In this numerical study an optimized trench film cooling design is determined using a Bayesian algorithm and neural network trained RANS model. Three objective functions were considered, the area-averaged film cooling efficiency, spatial standard deviation of film cooling efficiency and hot gas ingestion into the trench. Nine geometrical design parameters were varied to allow for a 3D trench shape and to find an optimal trench design based on the initial parametrization of the trench. Jet-engine like inflow boundary conditions with respect to turbulence intensity and length scales were applied. The investigated momentum ratios (I) were 1 and 8 at a main flow Reynolds number (Re_D) of 2500. For each design the steady state Reynolds Averaged Navier-Stokes (RANS) equations were solved using the commercial Computational Fluid Dynamics (CFD) code Ansys Fluent V2022 R1. The turbulence model coefficients of the generalized $k-\omega$ (GEKO) model were tuned to approximate the time-averaged 3D temperature field from a predictive Large Eddy Simulation (LES) and trained by a neural network to improve the prediction capability. The tuned GEKO model shows improved agreement with experimental data of a literature case compared to the standard GEKO model. With this tuned RANS model optimized trench designs are found and validated by additional LES's. The optimized designs include angled side walls to improve former trench designs, particularly in mitigating hot gas entrainment into the trench, which could be omitted almost entirely.

1. Introduction

The combustion process in gas turbines leads to high temperatures in the combustor and high pressure turbine which requires the application of film cooling techniques. Advances in film cooling would lead to lower maintenance costs for both combustor and turbine components. This is achieved by a reduced amount of coolant air in the turbine which increases the thermodynamic cycle efficiency. Various methods, such as internal convective cooling, external film cooling, and Thermal Barrier Coating (TBC), have been utilized to improve the cooling performance. This paper deals with external film cooling designs embedded in a TBC layer. Until today, mostly cylindrical and fan-shaped holes are used to create the coolant film [1,2]. A TBC-embedded trench can improve film cooling efficiency [3,4] and is visualized in Fig. 1.

However, as discussed and shown by [5–8] hot gas may be entrained into the trench leading to local heating at the metal wall which is not protected by the TBC. Furthermore, an early mixing of hot and cooling gas reduces the film cooling efficiency on the downstream wall, which has to be avoided. In the past, the main focus of studies on film cooling was to increase the adiabatic film cooling efficiency. Most numerical and experimental studies, including the trench design, focused on the investigation of the effect of one parameter variation like trench depth [9], width [10], pitch [11], trench shape (wave shaped [12], surface trenches [13]), trench outlet configuration (edge either sharp, beveled or filleted) [14], cylindrical or fan-shaped holes embedded in a trench [11] and trenches with compound angle holes [15]. Schreivogel et al. [16] performed a study to optimize the trench design further with respect to overall film cooling efficiency and standard deviation of the film cooling efficiency. They evaluated 42 trench designs with RANS simulations based on a Design Of Experiments (DOE). Subsequently, a meta model was created from this small data base to further optimize the design with a genetic algorithm. All trench designs featured a 2D contour because possible additive manufacturing methods were not considered.

Other optimization studies were conducted without trenches. As part of a parametric optimization the forward and lateral expansion angles of fan-shaped holes were varied. The test matrix

* Corresponding author.
E-mail address: l.fischer@unibw.de (L. Fischer).

https://doi.org/10.1016/j.ijheatmasstransfer.2023.124399

Nomenclature

Roman Symbols

BF	Blending function of the GEKO model
C	Free coefficient of the GEKO model
D	Film cooling hole diameter
dV	cell volume
DR	Density ratio
I	Momentum ratio
J	Observation J
k	Turbulent kinetic energy
P	Design parameter
q	Flow solution
Re	Reynolds number
r	Fillet radius
T	Temperature
Tu	Turbulence intensity
u, w	Axial and wall normal velocity component
V	Velocity magnitude
x, y, z	Cartesian coordinates

Greek Symbols

δ	Boundary layer thickness
$\Delta\bullet$	Difference of parameter e.g. η
ϵ	Dissipation rate of turbulent kinetic energy
η_T	η at the trench wall
Λ	Turbulence length scale
ρ	Density of the fluid
σ	Standard deviation of η
ω	Specific dissipation rate

Subscripts

aw	Adiabatic wall
c	Cold gas
i	Index
NW	Near wall
Mix	Free shear mixing
Max	Maximum
Sep	Separation
T	Trench wall
∞	Free-stream

Abbreviations

AMG	Algebraic Multigrid
CFD	Computational Fluid Dynamics
DOE	Design Of Experiments
GEKO	Generalized $k-\omega$
LES	Large Eddy Simulation
Param	Design Parameter
RANS	Reynolds Averaged Navier-Stokes
RSM	response surface model
SBES	Stress-Blended Eddy Simulation
ST	Schreivogel Trench
SIMPLEC	Consistent Semi-Implicit Method for Pressure Linked Equations
TT	Transverse Trench
UBC	Upper Confidence Bound
WALE	Wall-Adapting Local Eddy-Viscosity

consisted of 53 designs for 5 velocity ratios (265 simulations). RANS solutions were generated to test each design [17]. Round to slot holes were optimized in [18] with three design parameters. To construct a surrogate model a radial basis function neural network was applied to 25 CFD-evaluated designs. Subsequently, the optimal design point was searched for by a genetic algorithm as well. In another study, cylindrical film cooling holes were parameterized to change the shape from circular or elliptical to V-shaped holes based on discrete design parameter points. By applying the method of moving asymptotes, V-shaped holes with increased film cooling efficiency were found to be optimal [19]. Furthermore, an adjoint optimization was applied to improve the design of the fan-shaped hole [20]. No design parametrization had to be performed. In the adjoint approach the wall near the fan-shaped hole was adjusted in a way to improve the film cooling efficiency. Smooth vortex generators or ramps resulted upstream of the holes which were expected to be manufacturable by additive manufacturing.

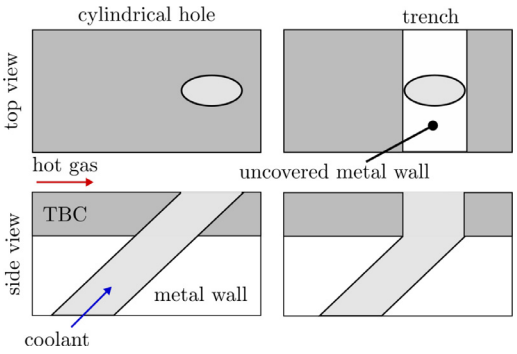

Fig. 1. Schematics of film cooling designs.

In all studies the realizable $k-\epsilon$ model with enhanced wall treatment was used. The authors were of the opinion that the model may not predict the correct absolute value but at least the trend. To improve the accuracy of the CFD approach, LES solutions were generated to optimize fan-shaped holes [21]. A Bayesian global optimization was performed based on a design of experiments resulting in 40 designs which were evaluated with LES. Nine more LES runs during the optimization were performed. The LES were performed on relatively coarse meshes (6 million elements) to reduce computational time.

The goal of this work was to improve the current trench designs with respect to three parameters. The aims were low hot gas ingestion (1) and superior film cooling efficiency (2) as well as homogeneous coolant distribution at the wall (3). For each of these targets a Bayesian optimization was performed. Thus, one novelty and focus in this current study includes advanced 3D film cooling trench designs with angled side walls, which may need to be manufactured additively [22,23]. In addition, former studies were conducted at low turbulence main flow conditions (0-6%) instead of high turbulence conditions which are to be expected in gas turbines [24]. Hence, turbulence intensities of around 20% with a length scale of up to 3.5 film cooling hole diameters were provided at the domain inlet during the design optimization process in the current study. The second novelty and emphasis in the study involve the utilization of a neural network-trained RANS turbulence model to enhance the accuracy of the film cooling prediction compared to the realizable $k-\epsilon$ model. For this an adjoint optimization to tune the GEKO model coefficients with respect to a high-fidelity LES solution was utilized. To the knowledge of the authors this was first time that this approach was used for film cooling simulations.

This article is structured as follows: First the approach to optimize the film cooling design is elucidated. This section includes the choice of optimizer algorithm, how the trench CAD model was parameterized and the CFD settings. The CFD section deals with the tuning of the GEKO model and its validation with LES and with experimental results of a low turbulence test case. Subsequently, the RANS and LES results of the trench design optimization at high turbulence boundary conditions are presented which are compared

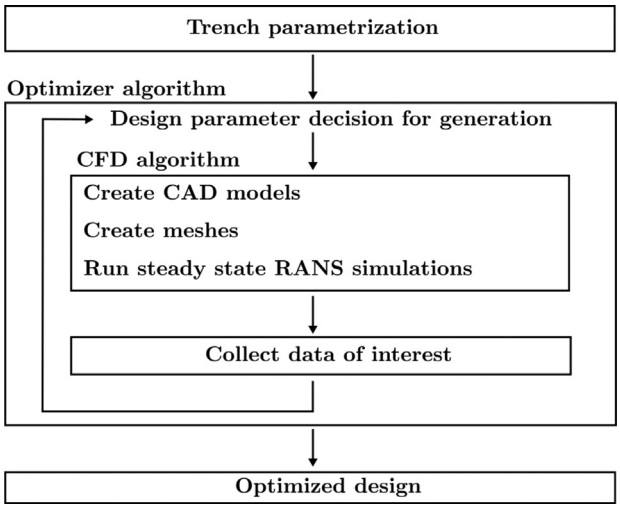

Fig. 2. Overview of the optimization procedure.

with results using a classic transverse trench and a former optimized trench design.

2. Design optimization

An overview of the design optimization procedure is given in Fig. 2. First, the shape of the trench is specified by parameterizing it. Next, the optimizer, here a parallelized Bayesian optimization algorithm, decides which designs are evaluated in this generation of designs. For each generation 20 designs were evaluated in parallel. Evaluating a design means performing a CFD simulation (CAD model creation and meshing, simulation and postprocessing). Each design was simulated for two momentum ratios. Subsequently, the data of interest for each CFD simulation is collected and fed back into the optimizer algorithm.

The objective functions to be optimized are three output parameters of the CFD simulations. The area-averaged film cooling efficiency of the trench walls (bottom and sides, $\overline{\overline{\eta}}_T$) and of the wall downstream of the trench ($\overline{\overline{\eta}}$) as well as the standard deviation of the film cooling efficiency of the downstream wall $\overline{\overline{\sigma}}$. The surface of interest for the downstream wall is shown in Fig. 6. The film cooling efficiency at the trench walls proved to be proportional to the hot gas mass flux entrained by the trench. The film cooling efficiency can be expressed as

$$\eta(x,y) = \frac{T_h - T_{aw}(x,y)}{T_h - T_c} \tag{1}$$

where T is the static temperature of the hot gas (h), coolant (c) and at the adiabatic wall (aw). The objective parameters for the optimization were then defined as:

$$\overline{\overline{\eta}} = \frac{\sum \eta_i(x,y) \cdot dA_i}{A} \tag{2}$$

$$\overline{\overline{\eta}}_T = \frac{\sum \eta_{T,i}(x,y) \cdot dA_{T,i}}{A_T} \tag{3}$$

$$\sigma = \sqrt{\frac{\sum \left(\eta_i(x,y) - \frac{\sum \eta_i(x,y)}{N}\right)^2}{N}} \tag{4}$$

in which dA are the surface elements (index: i) of the downstream or trench wall. The optimizer was searching for the minimum of each function by changing 9 trench design parameters. Therefore, 1-$\overline{\overline{\eta}}$ and 1-$\overline{\overline{\eta}}_T$ were used as optimizer parameter. This way all output values should reach a value as low as possible. The idea was to create a trench with low hot gas ingestion and improved lateral coolant distribution and high film cooling efficiency compared to other trench designs. In the following subsections each step of the optimization procedure is described in more detail.

2.1. Bayesian optimizer algorithm

To find the optimal film cooling trench design a computational budget equivalent to about 200 times 20 simultaneous CFD simulations was available. Therefore, CFD simulations were set up automatically based on 9 design parameters. To make the best out of the available computation time, an optimization algorithm was needed to choose future design parameters, also called hyperparameters, wisely. Evaluating the objective function for the trench design means generating a number of CFD solutions and computing a statistic from it. The objective function does not have an analytical form. Derivatives can only be approximated.

2.1.1. Requirements

Thus, the optimization algorithm has the following requirements:

1. search the hyperparameters space efficiently. It is satisfactory to find a near-optimal solution instead of the global minimum.
2. deal with a non-smooth optimization problem. If an invalid CAD design was created, a high value for the objective function will be reported (where a low value is optimal). Divergence during the CFD runs did not occur.
3. handle local minima in a way that the algorithm does not get stuck in them but instead continues to search elsewhere. This makes the optimization problem global.
4. run multiple simulations in parallel.
5. hyperparameters are constrained by upper and lower bounds.

The 'no free lunch theorem' [25] states that no optimization algorithm is better than another across all possible problems. That means prior to testing, it is unknown which optimization algorithm will perform best for a specific problem. Based on our requirements, some algorithms could immediately be disregarded: Multi-start algorithms need many evaluations and may not meet point 1. Any gradient-based algorithm may fail with point 2. Any local optimization algorithm does not meet point 3. Almost any algorithm can be implemented in some way to allow for point 4 and 5. Thus, five algorithms (Grid Search and Random Search, Nelder-Mead simplex method [26], DIRECT [27], Genetic Algorithm [28] and the Bayesian optimization) were considered. All fulfill point 2 to 5 but not all fulfill point 1.

The Bayesian optimization algorithm was chosen to optimize the design parameters for the film cooling trench because it uses the computational budget more efficiently than the other algorithms under consideration. It solves a secondary optimization problem to choose future design parameters. The Python package GPyOpt 1.2.6 [29] is an implementation of the Bayesian optimization algorithm and was chosen in this work. Adjustments to the code were necessary to offer interfaces to the in- and outputs of the CFD simulations. The following arguments are different from GPyOpt's default settings:

1. *domain* was used to handle the constraints on the design parameters.
2. *evaluator_type='thompson_sampling'* was chosen to select the different hyperparameters for a batch.
3. *batch_size* was used to adjust the batch size, and *initial_design_numdata* was set to the same value.

To test the optimizer, it was applied to two test functions (Rosenbrock and Rastrigin). These functions are both non-linear, smooth, and non-convex.

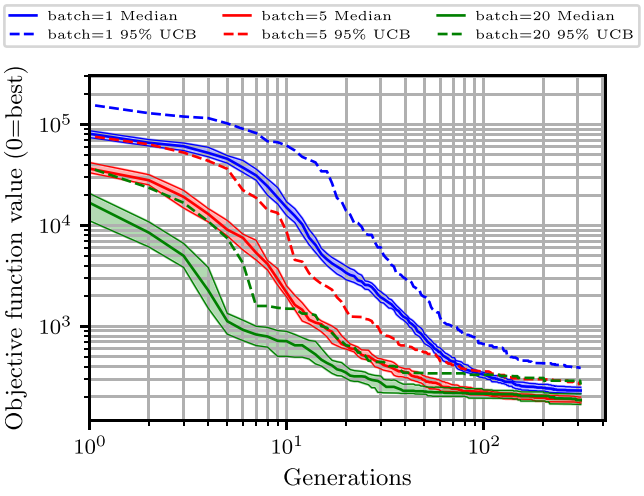

Fig. 3. Comparison of batch sizes for the 9D Rosenbrock function on the value of the objective function. The median and the upper confidence bound (UCB) are plotted over the generation number.

Hence, these functions offered to test local and global optimization qualities of the chosen Bayesian optimizer algorithm. A total of 568 runs, corresponding to about 1.4 million function evaluations, were performed for the test functions.

For each run one batch of initial data was generated, and then 310 generations were computed. One generation corresponds to a model update and then batch size many objective function evaluations.

2.1.2. Varying the batch size

To evaluate how well Thompson sampling works, three different batch sizes (1, 5 and 20) were compared for the 9-dimensional Rosenbrock function. A batch size of one means no evaluations are performed in parallel and Thompson sampling is not used. A lower batch size can outperform a higher batch size by chance despite being statistically worse. Multiple runs for each batch size were completed and two statistics for each batch size were computed and are shown in Fig. 3. The first statistic is the median which was chosen because it is less influenced by outliers than the arithmetic mean. The 95% upper confidence bound (UCB) is estimated with the 95th percentile of all runs of each batch size as the second statistic. 95% of all runs are estimated to be better (lower) than this bound. Fig. 3 shows that a higher batch size features a lower median and upper confidence bound at all generations than a lower batch size. The advantage is bigger initially and becomes less with increasing number of generations. For a low number of generations, having more function evaluations ensures a better performance. The chance of performing better with one evaluation versus 20 is low. Thus, the performance difference is very pronounced. For a higher number of generations, this advantage becomes smaller which shows the power of the Bayesian algorithm. A lower batch size with a lower number of function evaluations on which the surrogate is based on, still converged towards the global optimum. However, its performance was not as consistent. Assuming a normal distribution for the results, the standard deviation at generation 310 of batch size one was about 60% higher than for batch size 20. Further, even though the performance difference is not as pronounced at generation 310, a higher batch size still performed statistically better.

Already 70 generations with a batch size of 20 (20 designs for one generation) were almost as good as the 310 tested generations for both test functions. Since there were three objective functions (see Eqs. 2, 3 and 4) for the film cooling design optimization each objective function was evaluated for 71 generations. First, the optimization for increasing the film cooling efficiency was conducted. Subsequently, the film cooling efficiency in the trench (hot gas ingestion reduction) and at last the decrease of the standard deviation of the film cooling efficiency was optimized. For each optimizer restart the previous results were considered for the Bayesian model update.

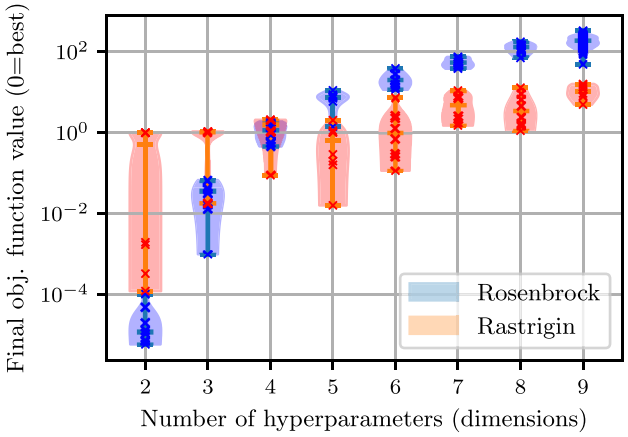

Fig. 4. Comparison of optimal solutions for different number of (design) parameters for Rosenbrock and Rastrigin functions.

2.1.3. Varying the number of design parameters

In this section the impact of the number of design parameters on finding an optimum with the Bayesian algorithm is evaluated. The number of design parameters was varied from 2 to 9 for the two test functions in Fig. 4. The translucent surface describes the distribution of the final value of the objection function depending on the test run. The influence of dimensionality can be seen very well for the Rosenbrock function. For a larger number of design parameters, the optimal solution found is farther from the true global optimum. The local search for the optimum within the flat valley becomes harder for higher dimensions. The Rastrigin function does show this trend as well, but less so. However, the found global minimum relative to the global maximum was 1% and 0.01% for the Rastrigin and Rosenbrock function in 9 dimensions and for lower dimensions it was even better. Thus, it can be concluded that the chosen Bayesian algorithm is well suited to get near the global optimum even for 9 dimensions. In the next sections the geometry and mesh generation as well as the details to the CFD simulations are given which evaluate the objective functions to find a new trench design.

2.2. Geometrical design parameters of the trench

The Ansys workbench was used to create the CAD models and meshes for the CFD simulations. The Design Modeler was chosen to build the CAD model of each trench design by defining variable parameters which were changed via workbench journal scripts. The design of the trench was varied through 9 parameters which are shown in Fig. 5 and described in Table 1. First, the parameters are described which give the basic shape of trench in the *xy*-plane (for more orientation please refer to Fig. 6). Parameter P_2 and P_3 determine the width of the trench near the centerline and at the outer pitch at the bottom of the trench. The trench can be tilted in the downstream direction by parameter P_4 to reduce recirculation regions in the trench. In addition, the trench depth (*xz*-plane) is varied with parameter P_5. The depth of the trenches varies between $0.5D$ and $0.75D$. The dimensions are non-dimensionalized by the diameter of the cylindrical film cooling hole with $D = 6$

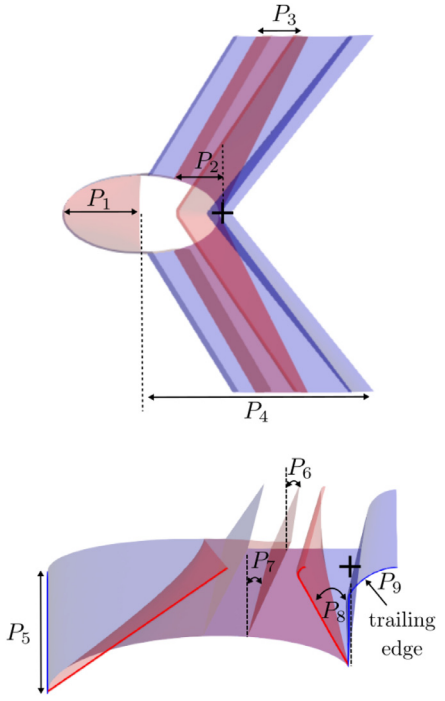

Fig. 5. Trench layout and variable geometry parameters. Top: top view (*xy*-plane); Bottom: Isometric view from the symmetry plane into the trench (close to *xz*-plane). Origin marked by black cross. The red and blue trench contours correspond to 2 different possible designs. (For interpretation of the references to colour in this figure legend, the reader is referred to the web version of this article.)

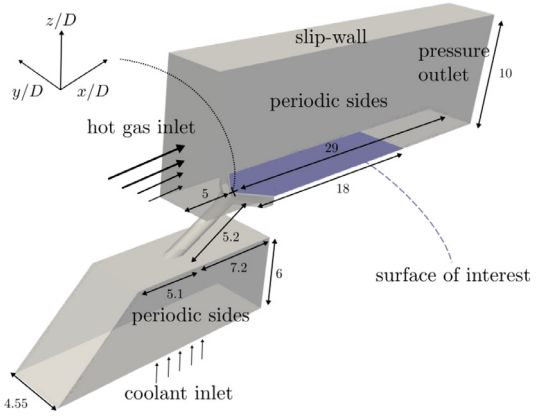

Fig. 6. Computational domain and boundary conditions. Dimensions are non-dimensionalized by the hole diameter.

mm. If the trench should be embedded into a thermal barrier coating (TBC) it needs to be shallow because of the limited thickness range of the TBC in real engines [30]. Hence, the maximum depth was limited to 0.75D which was used in the work of Schreivogel.

Additive manufacturing could allow for the trench walls to be tilted inwards of the trench. This is possible by the parameters P_1, P_6, P_7 and P_8. The intention with parameters P_1, P_6 and P_7 is to reduce the hot gas entrainment into the trench by tilting the leading edge (LE) and trailing edge (TE) of the trench walls. In addition, the downstream trench wall can be tilted by parameter P_8 to deflect the coolant to the left and right side of the trench to increase lateral spreading of the coolant. The parameter P_9 varies the fillet radius of the trench trailing edge to improve the coolant attachment to the downstream wall surface due to the Coanda effect, which increases the film cooling efficiency η as described in [14].

Table 1
Parameter range of the trench-shape specification.

Param.	Coord.	Min	Max	Description
P_1	x/D	0	1	hole closing length
P_2	x/D	0.6	0.9	trench width inside
P_3	x/D	0.6	1.6	trench width outside
P_4	x/D	1.3	3.3	distance hole center to TE
P_5	z/D	0.5	0.75	trench depth
P_6	-	5°	15°	wedge angle outside LE
P_7	-	5°	15°	wedge angle inside LE
P_8	-	20°	40°	wedge angle inside TE
P_9	r/D	0.04	0.25	fillet radius at trench TE

The edge perpendicular to the trailing edge (TE) of the trench has a fixed radius of $r/D = 0.16\overline{7}$ which vanishes towards the hole outlet.

2.3. Computational domain and mesh

The computational domain is depicted in Fig. 6 and dimensions are matching the experimental setup of Schreivogel et al. [16] to be able to validate the RANS and LES simulations. The surface of interest indicates the wall where η and σ were evaluated. The height of the main channel was 10D, which was sufficient to avoid acceleration effects on the main flow velocity after adding the cooling film mass flow. The axial location of the origin of the coordinate system (symbol **+**) was located at the downstream (trailing) edge of the film cooling hole. The origin was located in the center of the domain at the downstream wall. The inlet and outlet of the main channel were located 5D upstream and 29D downstream of the origin. The film cooling hole was inclined at an angle (α) of 30°. The hole length to diameter ratio was fixed to $5.16\overline{6}$ and the edge was sharp at the hole inlet to have the same geometrical inflow conditions as in the literature case [16]. However, one should note that Furgeson et al. [31] encountered feature deformation especially at the inlet and outlet of the hole when comparing as designed and as built designs for additively manufactured film cooling holes. Moreover, it was shown that for fan-shaped holes the measured overall effectiveness was reduced with the hole inlet fillet (due to feature deformation) compared to a sharp inlet because a fillet decreased inhole convection and jet mixing compared to when the inlet is sharp [32].

The Ansys mechanical mesher created the unstructured meshes with tetrahedral cells. The geometry described earlier was only created for half of the domain. First, a mesh for half of the domain was created. Second, this mesh was mirrored to create a symmetric mesh. This has the additional advantage of lower meshing runtime. A preliminary study with the realizable $k-\epsilon$ and standard GEKO model was conduced which showed that the whole domain needed to be simulated. Additionally, when considering an array of three film cooling holes, a similar trend was observed. Simulating only half of the domain with a symmetry plane led to different results which is in contrast to the statement of [16] who did CFD simulations with half a domain only. The tetrahedral growth rate was set to 10%. The final mesh setting featured 25 prism layers to resolve the boundary layer ($y^+ < 1$) which were created by the smooth transition algorithm with a transition ratio of 0.5 to provide similar cell volumes between the last inflation layer and adjacent tetra cells. Stair stepping was avoided. The typical first cell height in regions of high near wall velocity was of size $1.5e^{-4}D$.

2.4. CFD approach

This subsection describes the numerical settings for the RANS and LES, the boundary and initial conditions as well as the adjoint GEKO model tuning and validation.

2.4.1. Numerical settings

The steady state CFD simulations were run with Ansys Fluent. Its coupled algorithm solved the pressure based equation system based on the Reynolds-averaged Navier-Stokes (RANS) equations, energy equation and ideal gas equation. The gradients were computed with the Green-Gauss Node-Based method. The convective terms in the density, momentum, turbulent kinetic energy, specific dissipation rate and energy equations were discretized with the second-order upwind scheme. The continuity equation was discretized with the second-order scheme (central differencing scheme).

The pseudo transient approach with the default values for the explicit relaxation factors was employed to reach a converged state. A preliminary solution with first-order schemes was created for 1 through flow (main channel length divided by main flow velocity) before switching to the second-order schemes. Around 30 through flows of the domain were calculated corresponding to 1000 iterations. The pseudo time step for the first 400 iterations was set to $1e^{-3}$ s and was reduced to $1e^{-4}$ s for the remaining iterations to improve the convergence (Courant number of around 400). In addition, the mesh was once adapted on the fly to ensure a resolved viscous sub-layer ($y+ \leq 1$) at the wall for all solutions. The three parameters of interest were sampled at each iteration which showed a steady signal for the last 300 iterations while the locally scaled residuals were continuing to drop from $2.5e^{-5}$ to $1e^{-7}$.

The fluid properties of air were described with a piecewise polynomial for the specific heat, a linear expression for the thermal conductivity and the two coefficient law of Sutherland for the viscosity. The molecular weight had a constant value of 28.96 kg/kmol.

The GEKO turbulence model [33] accounted for the description of the Reynolds stress tensor. It is a flexible two equation model based on a $k-\omega$ formulation to cover a wide range of industrial applications. Up to six free coefficients can be adjusted to match a resolved CFD simulation or experimental data without impacting the basic calibration of the model. As described later, these coefficients were tuned in a way that the temperature field of the steady state GEKO solution becomes an approximate of the time-averaged temperature field from a reference LES solution. In the following the numerical settings for the LES simulations are elucidated.

The LES simulations were performed with Ansys Fluent 2022 R1. Similar numerical settings as in the simulation of a laid-back fan-shaped film cooling hole by Yang et al. [34] were applied. The pressure-velocity coupling was performed by the SIMPLEC algorithm as this led to a significant speedup (2x) compared to the coupled solver. The central differencing scheme for pressure, second-order upwind scheme for density and energy equation as well as the bounded central differencing scheme for the momentum equations were applied. The gradient calculations on the cell faces were based on the Green-Gauss node based method and the warped-face correction was selected. The time derivative terms were discretized with the bounded second-order implicit scheme and a fixed time step of $dt = 1e^{-6}$ s was chosen leading to a maximum Courant number of around 4. The starting solution was provided by a converged RANS solution. For initialization of the flow field 5 through flows and for determining the time average 3 through flow time spans were simulated. The subgrid-scale stresses resulting from the filtering operation were modeled by the Wall-Adapting Local Eddy-Viscosity (WALE) model [35] where the turbulent Prandtl number was set to 0.85 to model the subgrid-scale turbulent flux. The resolved turbulent kinetic energy was higher than 80%, as needed for a resolved LES [36].

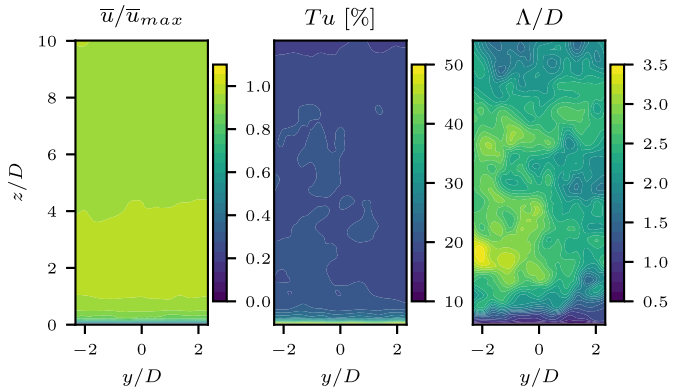

Fig. 7. Contours of the main stream velocity, turbulence intensity and length scale upstream of the film coolant injection at $x/D = -6$.

2.4.2. Initial and boundary conditions

The simulations were initialized from a quiescent velocity state and the temperature was set to the value of the coolant plenum inlet. The boundary conditions are visualized in Fig. 6. Possible backflow at the outlet which occured for the first iterations of the steady state simulations was prevented by setting the velocity vector to zero for the affected cells. The no-slip condition was used on all walls except at the top of the main channel (slip condition). The periodic boundary condition was applied on the lateral side patches. All walls were assumed to be adiabatic walls. The temperature at the test section inlet was set to $T_\infty = 373$ K and $T_c = 186.5$ K at the inlet of the cooling plenum. The resulting density ratio was $DR = 2$ which is common in gas turbines [2]. The ambient pressure was 0.96 bar in the reference experiment and thus set in the CFD as well. The velocity V_c at the coolant inlet was derived by the momentum ratios 1 and 8 defined by

$$I = \frac{\rho_c V_c^2}{\rho_\infty V_\infty^2} \quad . \tag{5}$$

Momentum ratios of 1 and 8 are common in the turbine and in the combustion chamber, respectively. The velocity vector at the coolant inlet points towards the hole to have comparable inflow conditions with the literature case of Schreivogel. Other investigations applied co- and crossflow inflow conditions (e.g. [37,38]). A maximum Mach number of 0.4 was reached inside the coolant hole due to the jetting effect [39] at a momentum ratio of 8. At the main flow inlet 2D contours of the time-averaged velocity, the turbulent kinetic energy k and the specific dissipation rate ω were interpolated. The free-stream Reynolds number based on the film cooling hole diameter was 2500. The contours were derived [40] from the temporal averaged velocity, turbulence intensity (Tu) and axial turbulence length scale (Λ) which are shown in Fig. 7. The maximum velocity in this contour is $\overline{u}_{\max} = 10.3$ m/s. The velocity components in the y and z direction were set to 0. The turbulent flow field resulted from an LES simulation of our thermal wind tunnel in which an active vortex generator was placed [24]. The mean velocity profile shows a homogeneous field with an area of higher velocity between $z/D = 2$–4. The turbulence intensity is around 20%, the axial turbulence length scale is very inhomogeneous and of an order of 1–3 film cooling hole diameters. These turbulence characteristics are common in gas turbines with rich or lean burners [24] and were applied during the design optimization. For the LES the spectral synthesizer was used to create a turbulent field from $k-\epsilon$ profiles which were derived based on the turbulence profiles in Fig. 7.

For the validation of the numerical approach (mesh independence study, GEKO model tuning and turbulence model validation) the numerical results were compared to experimental results

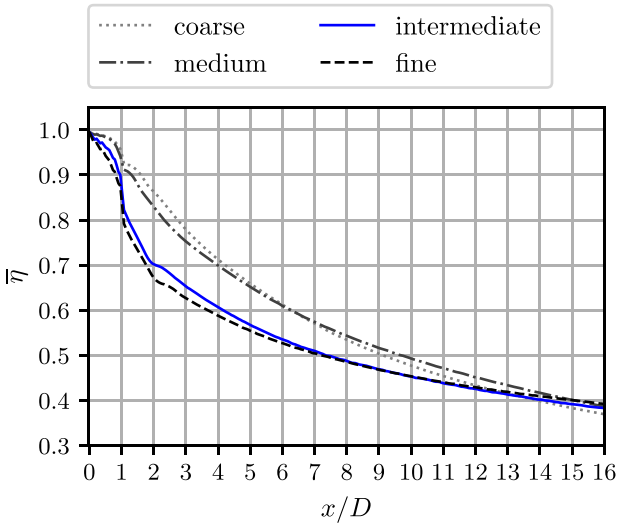

Fig. 8. Mesh independence study for the untuned GEKO model. Schreivogel trench at $I = 1$.

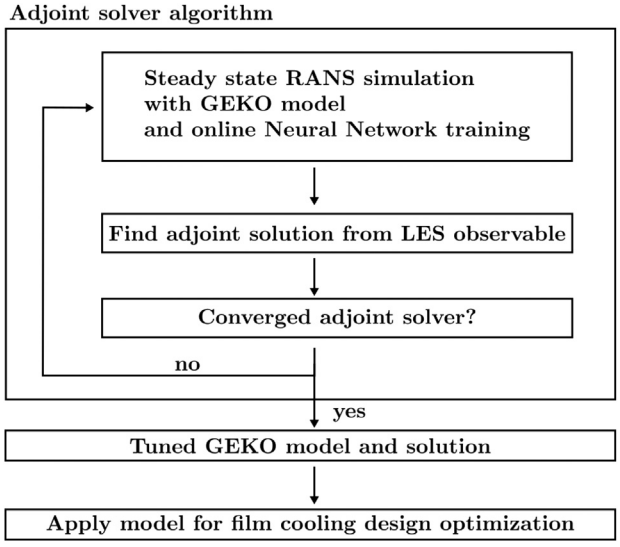

Fig. 9. Overview of the adjoint GEKO turbulence model tuning procedure.

of the Schreivogel trench at low turbulence conditions. For these cases the boundary conditions were adjusted as described in the following. A boundary layer velocity profile known from measurements at $u_\infty = 19.8$ m/s was applied at the domain inlet. It was approximated by a power-law profile [36] with

$$u(z) = u_\infty \cdot (z/\delta_{99})^{1/6} \quad , \; z \leq \delta_{99} \tag{6}$$

where z is the wall distance and u_∞ is the main-stream velocity of 19.8 m/s. The boundary layer thickness was $\delta_{99} = 1.08\overline{3}D$. The free-stream Reynolds number based on the jet diameter was 5000. The turbulence intensity was set to 1% and 5% at the main flow and coolant inlet. At both inlets the ratio of viscosity to turbulent viscosity was set to 10 which is the default value. From these parameters Ansys Fluent [40] calculated the turbulent kinetic energy k and the specific dissipation rate ω, needed for the turbulence model. For the LES simulations of the validation case no artificial turbulence was applied at the inlet because no information about the length scale was available and the turbulence intensity was deemed insignificant for the flow field.

2.4.3. Mesh study

To assess mesh independence and to study the effect of the prediction accuracy of the turbulence model the literature case of Schreivogel's optimized trench design [16] was chosen. The depth of the trench is 0.75D. Four meshes were tested with 4, 7, 10 and 24 million elements. Finer meshes were based on the coarse mesh. These were refined in the regions of interest, the film coolant hole, the trench, as well as the upstream and downstream region of the trench. Since the tuned GEKO model (described in the next section) is based on untuned GEKO model simulations, the mesh independence study was performed for the untuned GEKO model with default coefficients. The results of the mesh study are shown in Fig. 8. The laterally-averaged film cooling efficiency $\overline{\eta}$ is displayed over the axial distance from the film cooling hole outlet at $x/D = 0$ for $I = 1$. Mesh independence was reached for the intermediate mesh. In comparison, a mesh study using the realizable $k - \epsilon$ model with enhanced wall function already showed mesh independence for the coarse mesh (not shown). Thus, this model would not have required a high cell count and converges easily but it is also known for not correctly predicting the film cooling efficiency of fan-shaped holes [17] and holes embedded in trenches [16].

2.4.4. GEKO model tuning

The coefficient tuning of the GEKO model was performed to improve the quality of the numerical prediction. It was introduced in [41] to improve the prediction quality of aerodynamic objectives for cars. Two parameters C_{Sep} and C_{Mix} were tuned based on a scaled resolved Stress-Blended Eddy Simulation (SBES) solution. The chosen scalar observable was the drag coefficient. In the current study the target-volume-integral was the scalar observable and all four tuneable parameters [33] including the blending function (BF) were adjusted:

- C_{Sep}: Adjusts flow separation from smooth surfaces.
- C_{NW}: Adjusts wall shear stress.
- C_{Mix}: Adjusts the strength of mixing in free shear flows.
- BF: Deactivates C_{Mix} and C_{Jet} near the boundary layer.

As an example, increasing the value of the coefficient C_{Mix} is necessary because the RANS model tends to underpredict the mixing of coolant with the hot gas crossflow. This usually leads to an overestimation of the film cooling efficiency. Not including the blending function in the GEKO tuning process led to a worse agreement of RANS and LES solution compared to using all four parameters. Apart from the tuned parameters the default values for all parameters of the GEKO model were used (e.g. Prandtl number equal to 0.85). The optimization procedure was performed with the discrete adjoint solver of Ansys Fluent 2022 R1 and is described in Fig. 9.

For each iteration within the adjoint solver algorithm a well converged steady state RANS solution was found with the GEKO model. During each flow-iteration online neural network training was performed to correlate the underlying flow features with the turbulence model coefficients. Subsequently, the adjoint solver performed adjoint-iterations to tune the GEKO model parameters to reduce differences between the RANS temperature and the mean temperature field of the LES. Once the adjoint solver converged the trained GEKO model was available and applied for the trench design optimization study. During the CFD simulations of this study, the tuned GEKO model calculated the flow input features for each cell and derived specific values for the turbulence model coefficients from the neural network to improve the prediction. In the following more details are given for the adjoint solver and neural network training. Further information is to be found in the user-guide [40].

As a starting point of the adjoint solver a scalar-valued observation J (here: target-volume-integral) needed to be chosen which is defined as:

$$J(q, C) = \int (T_{i,RANS} - \overline{T}_{i,LES})^2 dV_i \tag{7}$$

in which dV_i is the cell volume, $T_{i,RANS} - \overline{T}_{i,LES}$ is the cell-based (index: i) temperature difference of the static temperature determined from the RANS solution and the temporal mean of the temperature from the LES. The goal of the adjoint solver was to minimize this integral. The observation J is a function of the flow solution $q(C) = (u, v, w, p, T, k, \omega)$ and the turbulence model coefficients C.

Subsequently, the same equations as for the flow solver were evaluated by the adjoint solver. To reduce memory requirements and iteration speed the partially coupled solver was chosen. Using matching numerical schemes between adjoint and flow solver yields the most accurate solution. However, due to stability issues the equations of the adjoint solver were discretized with first-order upwind schemes. Moreover, the Green-Gauss cell-based method was chosen as the gradient scheme.

The equation system was solved with an iterate AMG (Algebraic Multigrid) approach to find an approximate solution to the equations. The blended stabilization scheme was used to handle instabilities during the solving process. First, 300 iterations of the dissipation scheme were performed. Subsequently, 60 iterations of the residual minimization scheme with 120 modes, 30 recycled modes and 3 AMG iterations were performed. This routine was repeated (see Figure Fig. 9) until the residuals reached the specified threshold (1e-4). The optimization of the GEKO turbulence model took 30h on 336 CPU-cores.

The turbulence model parameters were optimized in online mode. This means that the training took place during each flow iteration (up to 1000 iterations with a pseudo time step size of $1e^{-4}$ s). This way the chosen turbulence model coefficients C_{Sep}, C_{NW} and C_{Mix} are calculated from flow input features through a neural network. The settings for the training are described in the following. The chosen activation function was Softsign. By default, the topology of the neural network was based on three hidden layers consisting of 24, 16, and 8 nodes for the first, second, and third layer. Six flow input features were selected: Non-equilibrium parameter, 2nd - 5th invariant and the length ratio. Moreover, the default design limits were chosen to only adjust each GEKO coefficient C within a certain threshold. The tuned model coefficients are available online [42].

2.4.5. Validation of tuned GEKO model and LES

Fig. 10 depicts the film cooling efficiency downstream of Schreivogel's trench at $I = 1$. The standard GEKO, tuned GEKO, LES and experimental results are shown. The standard GEKO model (in this form similar to the $k - \omega$ SST model) strongly overpredicts the film cooling efficiency. The tuned GEKO model shows a similar trend as the LES since it has been tuned to match this solution. The LES shows good agreement with the experiment. In the CAD model of the CFD simulations the edge was kept sharp. Differences are seen in the middle of the wall where the contours of the experiment are conical. This could be an effect due to ice formation during the experiments. LES with a CAD model including ice formation at the downstream edge of the trench lead to a conical shape of the film cooling efficiency as well (results not shown). All in all, the agreement of the LES with the experimental results is excellent. This indicates that the approach to tune the GEKO model with the LES solution is suitable.

For further validation, this tuned GEKO model was applied to a different trench design (the transverse trench as described in [16]) which is shown in Fig. 11. In a preliminary study high sensitivity of the downstream located trench edge was encountered of the film cooling efficiency. If the edge was kept sharp the film cooling efficiency strongly differed compared to a beveled edge which was also apparent in the experimental results of Schreivogel et al. [16,43]. In the current study it was decided to use a constant bevel with a length of 0.7 mm at an angle of 45° replacing the sharp edge in the CAD model of the transverse trench design to improve the agreement between CFD and experiment. The overprediction of film cooling efficiency in the LES is a consequence of the bevel whose length and angle do not match the experiment. The tuned GEKO model (tuned for the Schreivogel trench) reduces overprediction of the film cooling efficiency for the transverse trench compared to the standard GEKO model.

In Fig. 12 the laterally-averaged film cooling efficiency for both momentum ratios ($I = 1$ and 8) and trench designs are shown. The experimental results are also provided for reference but the results of the GEKO models should be compared to the LES result because of the uncertainty of the edge shape in the experimental trench design. The tuned GEKO model was optimized for a momentum ratio of ($I = 1$) and the results show a very good agreement with the LES for both designs. For the Schreivogel trench (ST) at $I = 8$ the model cannot follow the trend of the LES. However, the model offers a very good prediction of the film cooling efficiency of the transverse trench (TT) design at $I = 8$.

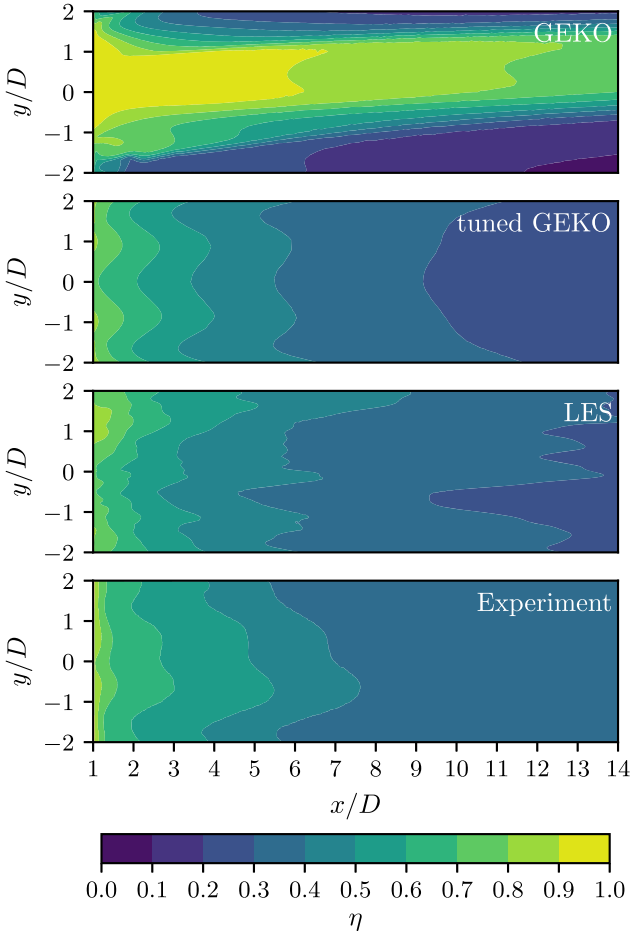

Fig. 10. Validation of the numerical approach by comparing the efficiency distribution at $I = 1$ of GEKO, tuned GEKO, LES and experimental[16] results of the Schreivogel trench (relatively sharp edge).

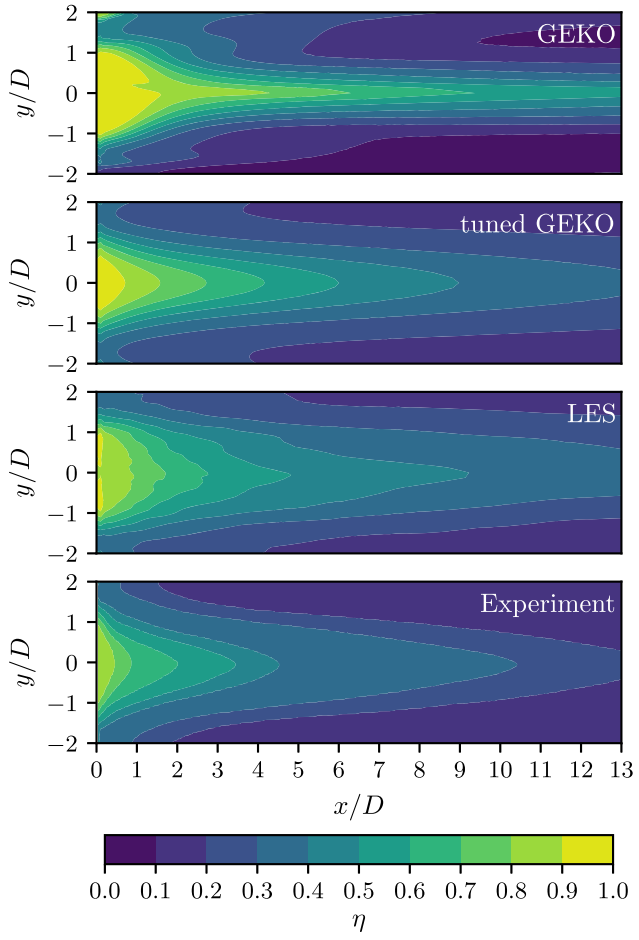

Fig. 11. Validation of the numerical approach by comparing the efficiency distribution at $I = 1$ of the tuned GEKO (tuned for the Schreivogel trench), LES and experimental[16] results of the transverse trench (beveled edge).

Table 2
Difference of the target parameters in percent (%) between the RANS (GEKO and tuned GEKO) and LES solution with low turbulence boundary conditions.

Case	Parameter	GEKO	tuned GEKO
ST $I = 1$	$\Delta\overline{\overline{\eta}}$	−25	5
	$\Delta\overline{\overline{\eta}}_T$	17	−5
	$\Delta\sigma$	−21	31
TT $I = 1$	$\Delta\overline{\overline{\eta}}$	11	7
	$\Delta\overline{\overline{\eta}}_T$	−12	25
	$\Delta\sigma$	−22	−5
ST $I = 8$	$\Delta\overline{\overline{\eta}}$	21	20
	$\Delta\overline{\overline{\eta}}_T$	12	−12
	$\Delta\sigma$	−37	1
TT $I = 8$	$\Delta\overline{\overline{\eta}}$	45	−7
	$\Delta\overline{\overline{\eta}}_T$	−3	7
	$\Delta\sigma$	−33	−22

Table 2 depicts the difference of the target parameters $\bullet$ (η, η_T, σ) defined as

$$\Delta\bullet = \frac{\bullet_{LES} - \bullet_{RANS}}{\bullet_{RANS}} \tag{8}$$

in percent (%) between the RANS (GEKO and tuned GEKO) and LES solution. This way the effect of the turbulence model on the optimizer parameters can be understood more clearly. With respect to the overall film cooling efficiency (η) the tuned GEKO model clearly outperforms the GEKO model (e.g. only 5–7% difference instead of 11–45% excluding the Schreivogel trench (ST) at $I = 8$). As seen before both models cannot predict the trend of the film cooling efficiency for the Schreivogel trench at $I = 8$ as both designs differ by $\approx 20\%$. Looking at the film cooling efficiency inside the trenches (η_T) the tuned model only offers an advantage over the standard GEKO model for the case it has been tuned to (ST at $I = 1$). Thus, it should be taken into account for the optimization results that the predicted designs with high film cooling efficiency inside the trench (ingestion) may be inaccurate for both tested momentum ratios. Regarding the homogeneity of the external film cooling efficiency represented by the variance σ, the tuned model shows improved prediction quality compared to the standard GEKO model. However, in two of the four tested cases the difference of σ with respect to the LES is greater than 22%.

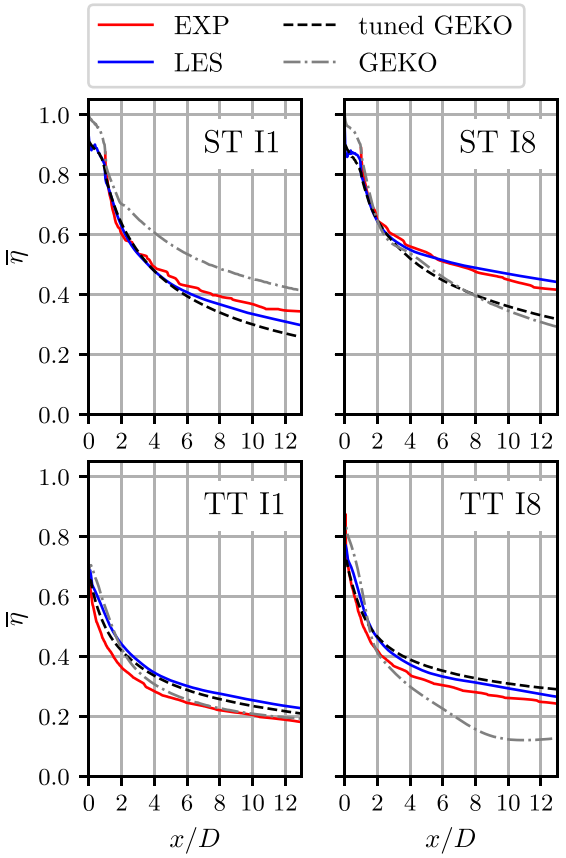

Fig. 12. Lateral averaged film cooling efficiency for Schreivogel trench (ST) and transverse trench (TT) at $I = 1$ and $I = 8$ at experimental conditions.

3. Design optimization results

In this section the results of the Bayesian optimization are discussed. First, an overview of the target parameters of all simulations is given. Next, the difference between tuned GEKO model and the WALE LES results under high turbulence boundary conditions are elucidated. Finally, two optimized designs are compared to the Schreivogel trench.

3.1. Overview of evaluated designs

The Bayesian optimizer was run with the previously defined parameters for the CFD case. Note, contrary to the low turbulence boundary conditions to tune the GEKO model the high turbulence boundary conditions (see Fig. 7) were applied at the inlet of the domain. An overview of all evaluated designs is given in Fig. 13.

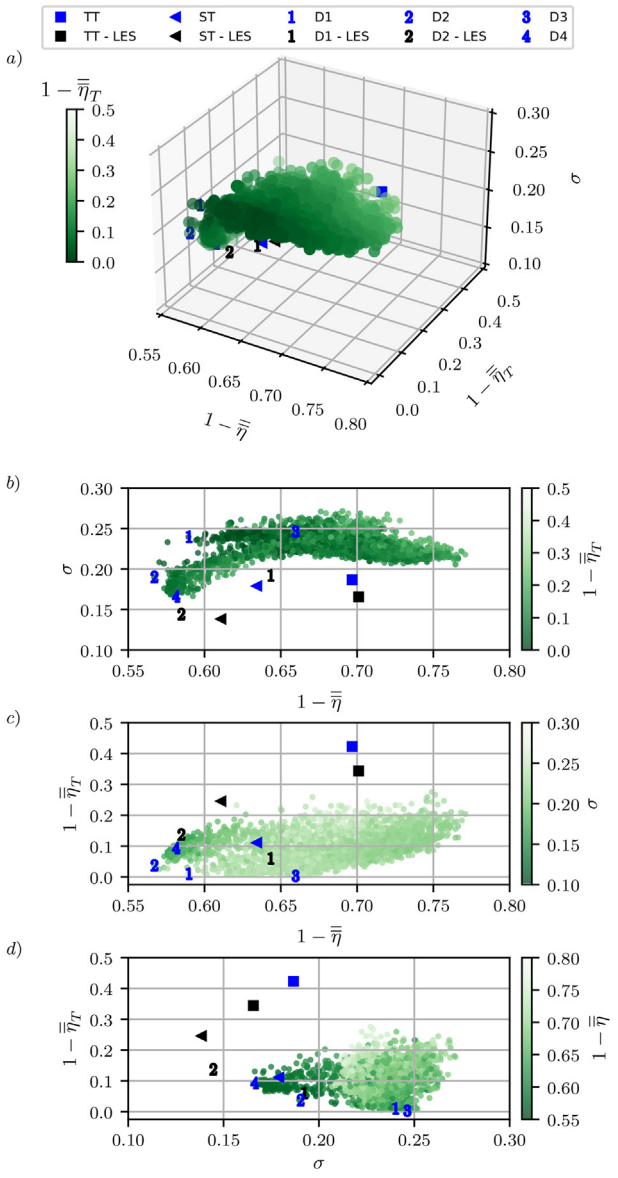

Fig. 13. Bayesian trench optimization results (green dots). The left corners in each subplot show the Pareto front (best designs). Four designs of interest have been chosen (D1 - D4). The classic transverse trench (TT) and Schreivogel trench (ST) are added for reference. The word LES implies that a design was reevaluated using LES. (For interpretation of the references to colour in this figure legend, the reader is referred to the web version of this article.)

Note, the target parameters, namely the film cooling efficiency parameters, are redefined as 1-$\overline{\overline{\eta}}$ and 1-$\overline{\overline{\eta}}_T$ to allow for the Pareto-front to be in the lower left corner of each subplot. The arithmetic mean values of the target parameters for both tested momentum ratios for each design are given. Results from the classic transverse trench (TT) and Schreivogel trench (ST) are added for reference. The word LES implies that a design was evaluated using LES. Four designs of interest were chosen from generation 56, 60, 138 and 151. The design with the highest film cooling efficiency was found at generation 56 (for $I = 8$) and 60 (for $I = 1$) within the 71 evaluated generations with the target to optimize for high efficiency. The designs are labeled D2 and D1, respectively. Subsequently, the optimizer was restarted to find a design (design from generation 138, labeled D3) with the highest film cooling efficiency within the trench (generations 72 to 142). Next, the optimizer's task was to find a design with the lowest possible standard deviation of the film cooling efficiency at the external wall (tested generations 143 to 213, labeled D4). It was successful doing so at generation 158.

Fig. 13 a) gives a 3D overview of the evaluated designs. The colorbar represents $1-\overline{\overline{\eta}}_T$ to get a feeling for the depth of the graph. Thus, in the lower left corner the Pareto front is represented by design D1, D2 and D4. The Schreivogel trench is located in the middle of the cluster and the transverse trench near the right upper corner indicating a poor design. Figs. 13 b)-d) offer 2D views of the target parameters of each design. The color represents the missing target parameter in each figure. In Fig. 13 b) designs D2 and D4 are to be found in the lower left corner which are the designs with the lowest standard deviation and highest film cooling efficiency. In Fig. 13 c) D1 and D2 are the designs with the highest film cooling efficiency and lowest hot gas ingestion represented by the cooling efficiency in the trench (1-$\Delta\overline{\overline{\eta}}_T$). In Fig. 13 d) D1 and D3 are the designs with the lowest hot gas ingestion. Design D4 offers the lowest hot gas entrainment. However, the design parameters led to a relatively tight gap between the trench walls (not shown) which may lead to increased difficulties during the manufacturing. In addition, the film cooling efficiency is not as high compared to Design D1 for which a very low ingestion, was predicted as well. Design D2 performs like the Schreivogel trench with respect to the standard deviation but outperforms it with respect to $\Delta\overline{\overline{\eta}}$ and $\Delta\overline{\overline{\eta}}_T$. Design D3 is predicted to outperform the Schreivogel trench in all three objective parameters. However, no design outperforms all designs in all of the three target parameters. Thus, a compromise was made to prefer design D1 and D2. Design D1 was of interest because the highest accuracy of the tuned GEKO model was shown to be for $I = 1$ at which this design had the highest film cooling efficiency. Moreover, this design has a high value for parameter $P1$ which should provide low ingestion into the trench thus offering a high film cooling efficiency within the trench. The tuned GEKO model showed to be less accurate with respect to ingestion (see e.g. Table 2), thus choosing design D1 with a nearly closed wall above the film cooling hole seemed to be a reasonable choice. Design D2 was as well of interested as it offered less ingestion compared to design D3 which had almost the same predicted ingestion as the Schreivogel trench.

3.2. Optimized designs of interest

Fig. 14 depicts the side and top views of Design D1 (top) and D2 (bottom). Both designs are compared to the Schreivogel design to underline the differences. Both optimized designs are similar. The biggest difference between these are parameter $P1$ and $P9$. Especially $P1$ allows for a reduction in hot-gas ingestion compared to the Schreivogel trench. The angled side walls of the trench ($P6$ and $P7$) further reduce hot gas entrainment. The reduced width of the trench near the hole exit ($P2$) contributes to this effect. The radius at the trailing edge due to $P9$ should lead to a better attachment of the coolant at the downstream wall. Parameter $P8$ may lead to a better distribution of the coolant into the sides of the trench by increasing the lateral spreading of the coolant. Both trench sides have a similar angle compared to the Schreivogel design ($P4$). However, the Schreivogel trench has a kink while the trenches in design D1 and D2 are continuing straight. The width of the trench at the end of the sides is similar to Schreivogel's design ($P3$). The depths of the trenches have a value of $P5 = 0.74D$ which is near the maximum of $0.75D$.

In Fig. 15 the results of the tuned GEKO model and LES with WALE model are shown for $I = 1$. The film cooling efficiency (η) is shown at the downstream wall and at the lower part of the trench. The upper half of the trench is colored in gray. The red contour indicates the non-dimensionalized wall normal velocity component w. A large area of this contour indicates high hot-gas ingestion. As mentioned earlier, the tuned GEKO model underpredicts ingestion.

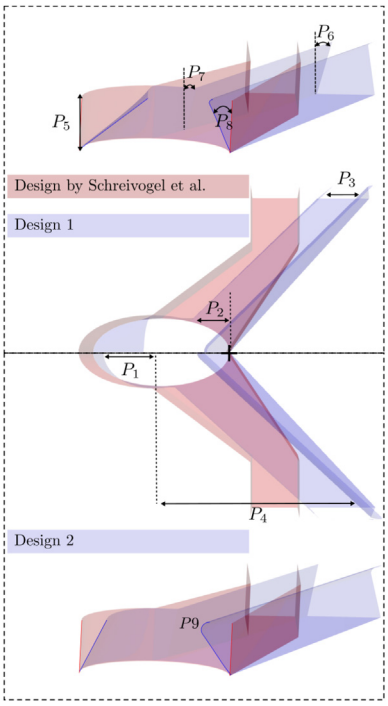

Fig. 14. Comparison of Design D1 and D2 with the Schreivogel design. Side and Top view (center).

The LES shows that for all designs the ingestion is increasing compared to the RANS results. The Schreivogel trench reduces entrainment of the hot gas due to the smaller trench area compared to the transverse trench. However, just above the hole exit hot gas entrainment cannot be stopped in these classic 2D-shaped trenches which are extruded in the wall normal direction only. Hot gas at the trench wall leads to local heating which has several disadvantages as elucidated in [5,8]. The bottom of the trench wall may not be covered by the thermal barrier coating which is a risk for material failure. Moreover, through thermal conduction the metal surface underneath the TBC may be heated. Due to the 3D design, the hot gas entrainment is strongly reduced by the new designs.

Comparing the LES to the RANS solution the ingestion area and velocity magnitude is increased in the LES, leading to lower film cooling efficiency at the trench wall. This also occurred for design D2. Design D1 is only affected at the side walls of the trench and the entrainment is much more limited in depth preventing hot gas reaching the bottom of the trench. At least this is the case for the time-averaged solution. The ingestion depth at instantaneous snapshots should be investigated in a future study. The qualitative agreement between the RANS and LES for the film cooling efficiency at the downstream wall is excellent for each tested design. In general the RANS results lead to an overprediction due to underpredicted mixing of the coolant and hot gas near the trailing edge of the trench but resulted in an underprediction of the film cooling efficiency further downstream. The asymmetry of the LES for design D2 did not change after doubling the number of through flows from 3 to 6 for the determination of the time average. The film cooling efficiency of the new designs is higher as for the clas-

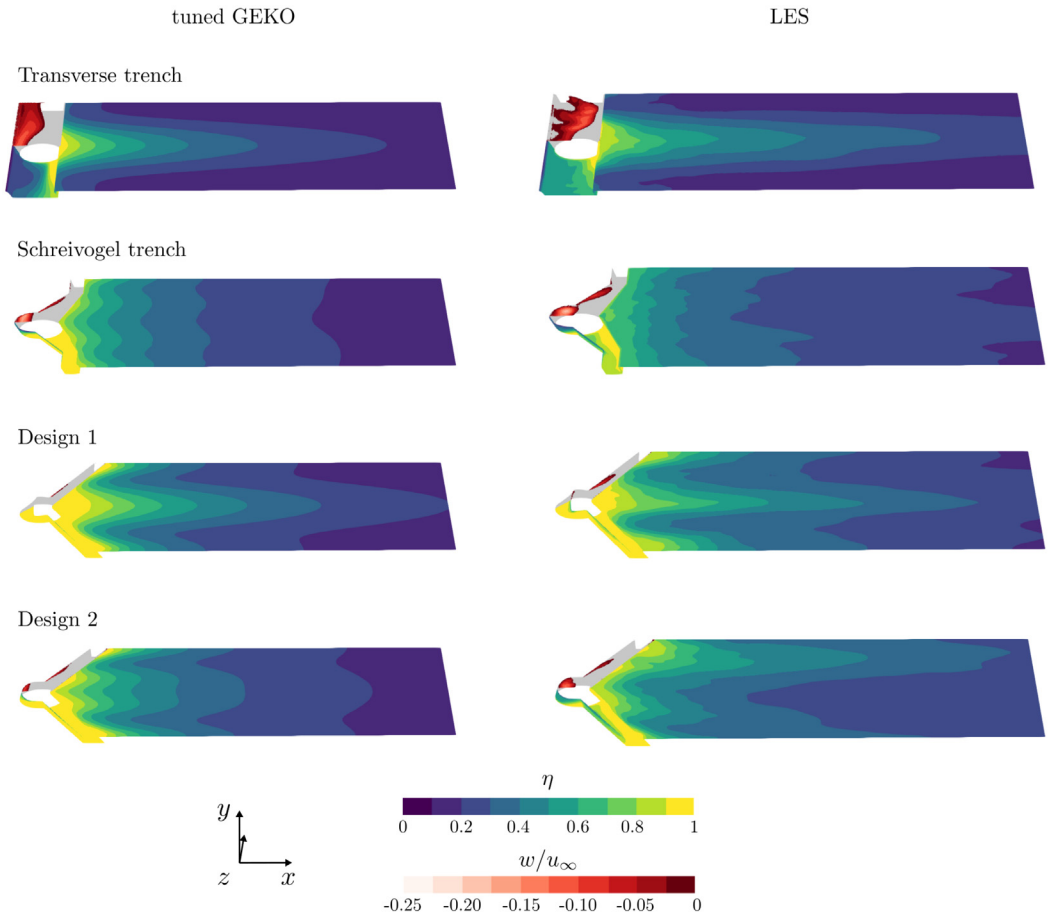

Fig. 15. Design 1 and 2 from the optimization process are compared to the classic transverse trench (TT) and Schreivogel trench (ST). Contours of the film cooling efficiency and ingestion for $I = 1$ with tuned GEKO model and WALE LES model are shown. Upper half of trench walls colored in gray.

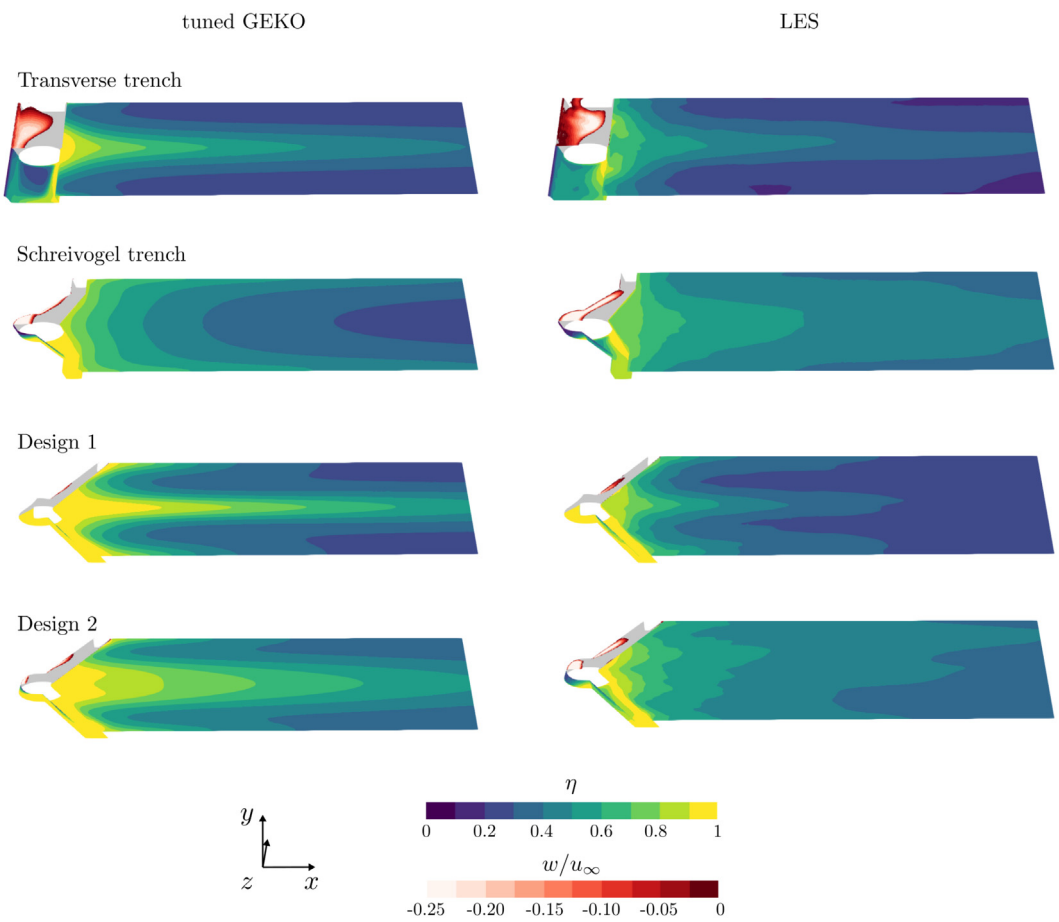

Fig. 16. Design 1 and 2 from the optimization process are compared to the classic transverse trench (TT) and Schreivogel trench (ST). Contours of the film cooling efficiency and ingestion for $I = 8$ with tuned GEKO model and WALE LES model are shown. Upper half of trench walls colored in gray.

sic designs. The standard deviation of the film cooling efficiency σ at the downstream wall is lower for the LES as the contours of the film cooling efficiency are smoother. The coolant distribution is the most homogeneous for the Schreivogel design compared to D1 and D2.

In Fig. 16 the results for $I = 8$ are shown. Compared to the GEKO RANS the hot gas ingestion is increased and the standard deviation is reduced for the LES. The limitations of the tuned GEKO model (tuned for $I = 1$ and applied for $I = 8$) becomes more visible here. The trend of the external film cooling efficiency is only well depicted for the transverse trench and design D1. Discussing the solutions of the external film cooling efficiency the Schreivogel trench and design D2 provide the best coolant coverage at the wall and have the lowest standard deviation (most homogeneous coolant distribution). However, design D1 reduces hot gas entrainment most effectively and prevents the hot gas reaching the ground of the trench wall. The design is not completely preventing ingestion but shows a huge reduction compared to the other three designs.

4. Conclusion

A trench design was parameterized with 9 design parameters to allow for a 3D design with the novelty of angled side walls. The CFD domains were prepared with high turbulence boundary conditions. The GEKO turbulence model was tuned using adjoint optimization with a neural network to match an LES result closely. Four coefficients of the GEKO model were tuned for low turbulence boundary conditions at a momentum ratio of 1. As a result, the tuned GEKO model coefficients resulted in a quantitatively improved prediction for the film cooling efficiency compared to when the standard GEKO coefficients were applied. In general, the tuned model overpredicted the standard deviation of the film cooling efficiency and underpredicted hot gas entrainment in comparison with the LES. The tuned GEKO model was able to show qualitatively the correct trend (film cooling efficiency distribution at the wall, especially for $I = 1$). The model became less accurate for high turbulence boundary conditions and for $I = 8$ (depending on the trench design). In general, at high turbulence boundary conditions the qualitative agreement of the predictions for $I = 1$ with the tuned GEKO and WALE LES model was excellent and the agreement at $I = 8$ was only given for two for the fours tested designs. The tuned coefficients of the model are available for the community [42] which may be useful for other wall bounded cooling flows.

A Bayesian optimizer was tested with two analytical test functions. If low computational power is available a batch size of 5 is recommended when the number of design generations is around 100 as it performed comparable as a batch size of 20. Moreover, the number of random samples should be around 5% of the total number of samples to provide the algorithm with a solid sample foundation to prevent testing of similar designs at the initial stage. The optimizer was applied to the CFD set-up where the target parameters were averaged from the results of the tested momentum ratios. The optimizer showed to be suitable for this kind of optimization problem because it found better designs when a new target parameter ($\Delta\overline{\overline{\eta}}$, $\Delta\overline{\overline{\eta}}_T$, σ) was chosen and tested a wide variety of designs parameter combinations (within around 4000 designs tested overall). Thus, we are confident that a near optimal design

with the RANS approach within the 71 design generations per objective parameter were found.

Four designs were presented:

1. Design 1 is the design with the highest value for $\Delta\overline{\overline{\eta}}$ at $I = 1$ and especially with low predicted ingestion.
2. Design 2 performs like the Schreivogel trench with respect to the standard deviation but outperforms it with respect to $\Delta\overline{\overline{\eta}}$ and $\Delta\overline{\overline{\eta}}_T$.
3. Design 3 is better than Schreivogel trench in all 3 objective parameters but was not further tested as it had a similar high hot gas ingestion.
4. Design 4 has the lowest hot gas entrainment. However, the design parameters lead to a relatively narrow trench (manufacturability) and the film cooling efficiency was not as high compared to Design 1.

There was no design which outperformed all other designs with respect to all three optimized parameters. We think that the main focus should be the hot gas entrainment reduction to offer a save alternative to the classical cylindrical and fan-shaped cooling hole without trenches.

The design optimization process could be improved to find a better trench design than the ones suggested. The GEKO model tuning should be performed for high turbulence boundary conditions and also for each tested momentum ratio. In general, more parameters could be added to parameterize the trench, for example allow for the trench wall to change direction (like it was possible for the Schreivogel trench). In addition, a fan-shaped hole could be combined with the trench instead of a pure cylindrical one. Design 1 to 4 could be further enhanced by performing an adjoint design optimization as shown in e.g. [20] in which no further parametrization of the trench design is needed. Instead of only focusing on the film cooling efficiency, the heat transfer coefficient and thus the resulting net heat flux reduction could be investigated as well. Finally, the unsteady flow fields of the suggested designs should be investigated to evaluate the mechanism of hot gas entrainment and how it affects the temperature at the trench wall over time at discrete times. A high turbulent periodic boundary condition representing e.g. periodic blade wakes or combustion processes instead of a digital filter could be applied to make the boundary condition more realistic.

Declaration of Competing Interest

The authors declare the following financial interests/personal relationships which may be considered as potential competing interests: Lukas Fischer reports financial support was provided by Deutsche Forschungsgemeinschaft (DFG). Michael Pfitzner reports financial support was provided by ITIS e.v. Sillvya Jeyaseelan reports financial support was provided by Erasmus and STIBET III.

CRediT authorship contribution statement

Lukas Fischer: Writing – original draft, Writing – review & editing, Data curation, Software, Funding acquisition, Investigation, Methodology, Project administration, Supervision. **Dominik James:** Software, Methodology, Writing – review & editing, Data curation. **Sillvya Jeyaseelan:** Investigation, Writing – review & editing, Data curation. **Michael Pfitzner:** Funding acquisition, Writing – review & editing, Project administration, Supervision.

Acknowledgments

Thanks to CADFEM for supporting us with the GEKO model tuning, CAD and mesh generation. Thanks to our colleagues from UniBw M: Axel Buck for his support on the digitization of Schreivogel's experimental 2D data of the film cooling efficiency to determine correct lateral averaged plots. Junsu Shin for his preliminary investigation of optimizer algorithms. The work was sponsored by the Deutsche Forschungsgemeinschaft (DFG project number PF 443/7-1). Sillvya Jeyaseelan thanks STIBET III from UniBw M and Eramus for support of this work. Michael Pfitzner thanks ITIS e.V. for support of part of this work. We acknowledge the financial support by the Universität der Bundeswehr München. The support is gratefully acknowledged.

References

[1] R.S. Bunker, A review of shaped hole turbine film-cooling technology, J Heat Transfer 127 (4) (2005) 441–453, doi:10.1115/1.1860562.
[2] D.G. Bogard, K.A. Thole, Gas turbine film cooling, J. Propul. Power 22 (2006) 249–270, doi:10.2514/1.18034.
[3] T. Wang, S. Chintalapati, R.S. Bunker, C.P. Lee, Jet mixing in a slot, experimental thermal and fluid science, 22 (1) (2000) 1–17, doi:10.1016/S0894-1777(00)00010-8.
[4] R.S. Bunker, Film cooling effectiveness due to discrete holes within a transverse surface slot, Turbo Expo 2002, Parts A and B, ASMEDC, Amsterdam, The Netherlands 3 (2002) 129–138, doi:10.1115/GT2002-30178.
[5] F.T. Davidson, J.E. Dees, D.G. Bogard, An experimental study of thermal barrier coatings and film cooling on an internally cooled simulated turbine vane, in: in: Proceedings of ASME Turbo Expo 2011, ASME, Vancouver, British Columbia, Canada, 2011, pp. 559–570, doi:10.1115/GT2011-46604.
[6] B. Kross, M. Pfitzner, Numerical and experimental investigation of the film cooling effectiveness and temperature fields behind a novel trench configuration at high blowing ratio, Heat Transfer, Parts A and B, American Society of Mechanical Engineers Digital Collection, Copenhagen, Denmark, 2012 41197–1208. doi:10.1115/GT2012-68125.
[7] P. Schreivogel, Aerothermodynamische Untersuchung von Filmkühlgeometrien für brennkammertypische Ausblaseraten, Ph.D. thesis, Neubiberg, 2015 Ph.D. thesis.
[8] L. Fischer, A. Sanchez, F. Schleich, F. Feller, R. Raffelt, M. Pfitzner, Conjugate heat transfer of cylindrical and trenched film cooling designs with array jet impingement, American Society of Mechanical Engineers Digital Collection, Rotterdam, Netherlands 6AT12A011 (2022), doi:10.1115/GT2022-80810.
[9] Y. Lu, S. Ekkad, Predictions of film cooling from cylindrical holes embedded in trenches, in: 9th AIAA/ASME joint thermophysics and heat transfer conference, American Institute of Aeronautics and Astronautics, San Francisco, California (2006), doi:10.2514/6.2006-3401.
[10] J.R. Dorrington, D.G. Bogard, R.S. Bunker, Film effectiveness performance for coolant holes imbedded in various shallow trench and crater depressions, American Society of Mechanical Engineers Digital Collection (2009) 749–758, doi:10.1115/GT2007-27992.
[11] H.A. Zuniga, J.S. Kapat, Effect of increasing pitch-to-diameter ratio on the film cooling effectiveness of shaped and cylindrical holes embedded in trenches, Heat Transfer, Parts A and B, American Society of Mechanical Engineers Digital Collection, Orlando, Florida, USA 3 (2010) 863–872, doi:10.1115/GT2009-60080.
[12] J.-s. Wei, H.-r. Zhu, C.-l. Liu, H. Song, C. Liu, T. Meng, Experimental study on the film cooling characteristics of the cylindrical holes embedded in sine-wave shaped trench, American Society of Mechanical Engineers Digital Collection, Seoul, South Korea V05CT19A017 (2016), doi:10.1115/GT2016-56856.
[13] K.V. Rao, J.S. Liu, D.C. Crites, L.A. Tapia, M.F. Malak, G. Sujatha, S. Balamurugan, Enhanced film cooling effectiveness with surface trenches, Heat Transfer, American Society of Mechanical Engineers Digital Collection, San Antonio, Texas, USA 3B (2013), doi:10.1115/GT2013-94530. V03BT13A017
[14] H.I. Oguntade, G.E. Andrews, A.D. Burns, D.B. Ingham, M. Pourkashanian, Improved trench film cooling with shaped trench outlets,, J Turbomach 135 (2) (2013) 021009, doi:10.1115/1.4006606.
[15] J. Li, J. Ren, H. Jiang, Film cooling performance of the embedded holes in trenches with compound angles, American Society of Mechanical Engineers Digital Collection, Glasgow, UK (2010) 1415–1424, doi:10.1115/GT2010-22337.
[16] P. Schreivogel, B. Kross, M. Pfitzner, Study of an optimized Trench Film Cooling Configuration Using Scale Adaptive Simulation and Infrared Thermography, in: in: Proceedings of ASME Turbo Expo 2014, American Society of Mechanical Engineers, Dõsseldorf, Germany, 2014, p. 11.
[17] F.B. Jones, D.W. Fox, T. Oliver, D.G. Bogard, Parametric optimization of film cooling hole geometry, Heat Transfer Combustors; Film Cooling, American Society of Mechanical Engineers, Virtual, Online 5A (2021), doi:10.1115/GT2021-59326. V05AT12A013
[18] Y. Huang, J.-z. Zhang, C.h. Wang, Shape-optimization of round-to-slot holes for improving film cooling effectiveness on a flat surface, heat and mass transfer, (2018), 54, (6) 1741–1754, doi:10.1007/s00231-017-2272-4.
[19] A. Madrane, H. An, J. Leng, M. Schaenzer, M.Q. Pham, G. Bourgeois, .A. Shanian, D. Pasini, Shape optimization of inclined hole for enhanced film-cooling performance using discrete adjoint method, Int. J. Therm. Sci. 158 (2020) 106542, doi:10.1016/j.ijthermalsci.2020.106542.
[20] F.B. Jones, T. Oliver, D.G. Bogard, Adjoint optimization of film cooling hole geometry, in: volume 5A: heat transfer-combustors; film cooling, American Soci-

ety of Mechanical Engineers, Virtual, Online (2021), doi:10.1115/GT2021-59332. V05AT12A014
[21] S. Agarwal, L. Gicquel, F. Duchaine, N. Odier, J. Dombard, D. Bonneau, M. Slusarz, Large Eddy Simulation Based Optimization of a Fan-Shaped Cooling Hole Geometry to Enhance Cooling Performance, 2022, V06AT12A007.
[22] C.K. Stimpson, J.C. Snyder, K.A. Thole, D. Mongillo, Effectiveness measurements of additively manufactured film cooling holes, J Turbomach 140 (1) (2018), doi:10.1115/1.4038182.
[23] A. Wildgoose, K. Thole, P. Sanders, L. Wang, Impact of additive manufacturing on internal cooling channels with varying diameters and build directions, J Turbomach 143 (2021) 1–52, doi:10.1115/1.4050336.
[24] L. Fischer, M. Straubwald, M. Pfitzner, Analysis of large eddy simulations and 1D hot-wire data to determine actively generated main flow turbulence in a film cooling test rig, J Turbomach 144 (11) (2022), doi:10.1115/1.4054778.
[25] D. Wolpert, W. Macready, No free lunch theorems for optimization, IEEE transactions on evolutionary computation, conference Name: IEEE Transactions on Evolutionary Computation 1 (1) (1997) 67–82, doi:10.1109/4235.585893.
[26] F. Gao, L. Han, Implementing the nelder-mead simplex algorithm withadaptive parameters, Comput Optim Appl 51 (1) (2012) 259–277, doi:10.1007/s10589-010-9329-3.
[27] D. Jones, J. Martins, The DIRECT algorithm–25 years later, J. Global Optim. 79 (2021) 521–566, doi:10.1007/s10898-020-00952-6.
[28] J.H. Holland, Adaptation in Natural and Artificial Systems - An Introductory Analysis with Applications to Biology, Control, and Artificial Intelligence, MIT press, 1992.
[29] T.G. authors, GPyOpt: A Bayesian Optimization framework in Python, 2016, (????).
[30] F.T. Davidson, D.A. Kistenmacher, D.G. Bogard, Film Cooling with a Thermal Barrier Coating: Round Holes, Craters and Trenches, in: in: Proceedings of ASME Turbo Expo 2012, ASME, Copenhagen, Denmark, 2012, pp. 1757–1768.
[31] M.T. Furgeson, E.M. Veley, C. Yoon, D. Gutierrez, D.G. Bogard, K.A. Thole, Development and evaluation of shaped film cooling holes designed for additive manufacturing, American Society of Mechanical Engineers Digital Collection, Rotterdam, Netherlands (2022), doi:10.1115/GT2022-83201. V06AT12A041
[32] E.M. Veley, K.A. Thole, M.T. Furgeson, D.G. Bogard, Printability and Overall Cooling Performance of Additively Manufactured Holes With Inlet and Exit Rounding, 2022, 145, 3,031017, doi:10.1115/1.4056389.
[33] F.R. Menter, R. Lechner, A. Matyushenko, Best Practice: Generalized k-omega Two-Equation Turbulence Model in ANSYS CFD (GEKO), tech. rep. version 1.00, 2019.
[34] L. Yang, F. Satta, D. Barsi, P. Zunino, Y. Luan, Numerical investigation of laid-back fan-shaped film cooling holes with large eddy simulation, American Society of Mechanical Engineers, Rotterdam, Netherlands (2022), doi:10.1115/GT2022-83961. V06AT12A045
[35] N. Franck, F. Ducros, Subgrid-Scale Stress Modelling Based on the Square of the Velocity Gradient Tensor, flow turbulence and combustion, 1999, 62, 3,183–200, doi:10.1023/A:1009995426001.
[36] S.B. Pope, Turbulent flows, 7th Edition, Cambridge University Press, Cambridge, UK (2010).
[37] C. Yoon, D. Gutierrez, M.T. Furgeson, D.G. Bogard, Evaluation of adjoint optimized hole - part II: parameter effects on performance, Heat Transfer-Combustors; Film Cooling, American Society of Mechanical Engineers Digital Collection, Rotterdam, Netherlands, 2022 6A. doi:10.1115/GT2022-82726.
[38] E. Lundburg, S. Lynch, K. Liu, H. Xu, M. Fox, The effect of diffuser shape for film cooling holes with constant expansion angles and area ratio, Heat Transfer - Combustors; Film Cooling, Vol. Volume 6A: Heat Transfer - Combustors; Film Cooling, American Society of Mechanical Engineers, Rotterdam, Netherlands 6A (2022), doi:10.1115/GT2022-81520. V06AT12A016
[39] J.H. Leylek, R.D. Zerkle, Discrete-jet film cooling: a comparison of computational results with experiments, J Turbomach 116(1994) 3. doi:10.1115/1.2929422358-368.
[40] Ansys, Ansys Fluent Users's Guide 2022 R1, ANSYS, inc, canonsburg, PA, 2022.
[41] H. Wu, H. Zhou, S. Xu, C. Ren, C. Quian, .T. Jadhav, Adjoint-based model tuning and machine learning strategy for turbulence model improvement, Detroit, Michigan, USA (2022) 01–0899, doi:10.4271/2022-01-0899.
[42] L. Fischer, M. Pfitzner, Providing adjoint optimized GEKO model coefficients for film cooling predictions of trench designs, Mendeley Data V1 (2023), doi:10.17632/5f7xcv8dgv.1.
[43] P. Schreivogel, M. Pfitzner, Heat-transfer-measurements-downstream-of-trenched, J Turbomach 138 (3) (2016) 031003, doi:10.1115/1.4031919.